

Phonon-phonon coupling in bismuth vanadate over a large temperature range across the monoclinic phase

Christina Hill

*Materials Research and Technology Department, Luxembourg Institute of Science and Technology,
41 rue du Brill, L-4422 Belvaux, Luxembourg and
University of Luxembourg, 41 rue du Brill, L-4422 Belvaux, Luxembourg*

Georgy Gordeev and Mael Guennou

University of Luxembourg, 41 rue du Brill, L-4422 Belvaux, Luxembourg
(Dated: June 9, 2023)

In this work we study phonon-phonon coupling in bismuth vanadate (BiVO_4), known for its second-order transition involving a variety of coupling mechanisms. Using Raman spectroscopy as a probe, we identify two optical coupled phonon modes of the VO_4 tetrahedron and study them by varying light polarization and temperature. The coupling manifests in non-Lorentzian line-shapes of Raman peaks and frequency shifts. We use theoretical framework of coupled damped harmonic oscillators to model the coupling and capture the phenomena in the temperature evolution of the coupling parameters. The coupling is negligible at temperatures below 100 K and later increases in magnitude with temperature until 400 K. The sign of the coupling parameter depends on the light polarization direction, causing either phonon attraction or repulsion. After 400 K the phonon-phonon coupling diminishes when approaching phase transition at which the phonon modes change their symmetry and the coupling is no longer allowed.

INTRODUCTION

Raman spectroscopy is a powerful technique to study lattice dynamics in ferroic oxides. In these materials, the phonon frequency strongly depends on external parameters such as temperature or pressure as well as on the order parameter for example the strain in the material. In order to determine the phonon frequency precisely a proper model to describe the line-shape of the phonon mode should be used. Typically, Raman bands are modelled by a Lorentzian function derived from the classical damped harmonic oscillator model in the approximation of low damping. The eigenfrequency is an important parameter to follow one particular phonon mode across the phase transition. In practice, various phenomena may lead to a deviation from a perfect Lorentzian line-shape: Gaussian like broadening due to instrumental effects [1, 2], the Doppler broadening in gases [3], the superimposition of Raman bands as in silicate glass[4], a strong anharmonic potential of atomic bands[5] as in ZnO [6] and in PbTiO_3 [7] or sample related effects observed for example in nanoparticules [5, 8–10], graphene and related systems [11, 12] or in polymers[13]. Another source for deviations from Lorentzian line-shape are coupling effects of various kind, i.e. when the system cannot be reduced to as set of independent oscillators. Coupling between two phonon bands is discussed in literature for quartz [14], BiTO_3 [15] and AlPO_4 [16, 17]. In ferroelectric KPD (KH_2PO_4) [18] and in the arsenates CsH_2AsO_4 and KH_2AsO_4 [19], proton-phonon coupling causes the deviation from a Lorentzian line-shape. Another widely discussed phenomenon is the coupling between one phonon and a broad continuum [20–23] in literature referred to as Auger-like resonant interference[20], Fano-interference [22, 23] or Breit-Wigner-Fano coupling [22, 24–27]. Coupling effects typically cause an asymmetric line-shape. In that case, the eigenfrequency no

longer converges with central frequency of the Raman mode. Modeling correctly the Raman line-shape is key to extract the eigenfrequency and therefore identify the Raman mode correctly.

The coupled damped harmonic oscillator (coupled oscillator) model has first been introduced by Barker and Hopfield.[28] They successfully applied it to explain the dielectric properties of various perovskites. Later, Scott[16], Zawadowski and Ruvalds [29], used the Green's formalism to derive a more generalized form to model phonon-phonon coupling in AlPO_4 . Katiyar et al. [19] and She et al. [18] then applied the Greens formalism for proton-phonon coupling in KH_2AsO_4 (KDA) and KH_2PO_4 (KDP), respectively. The coupling between phonon modes is a temperature induced effect and Chaves *et al.* [15] showed that only modes of same symmetry can couple. While the coupled oscillators model is known, its implementation can be challenging and misleading. In many cases, multiple solutions provide a good fit to the data leading to very different physical conclusions. The implementation of physical meaningful constraints on the modeling parameters is a key to overcome this problem. In the literature, constraining the complex coupling parameter assuming either pure real [15, 18, 19, 30] or pure imaginary [31, 32] coupling has been widely used. However, the physical correctness of the coupling parameters needs to be carefully revised. This can be done by fitting the line-shape of data measured at many temperatures (or pressures or electric fields). However there are not many examples in the literature where this has been done. BiVO_4 is a nice example to study effects of phonon-phonon coupling since it is well known for the phase transition driven by a B_g optical soft mode (tetragonal) coupled to an acoustic mode.[33, 34] The phase transition in BiVO_4 is classified as 2^{nd} order from high temperature tetragonal phase (space group $I4_1/a$) to a low temperature monoclinic

phase (space group $C27c$, most commonly described in non-standard setting $I2/a$), also referred to as Scheelite and Fergusonite structures respectively. The Raman active modes are known from standard symmetry analysis and they have been successfully assigned.[34, 35] Their frequency shifts with temperature and pressure across the phase transition have been reported.[35] However, we observed line-shape asymmetries of the vibration modes of the VO_4 tetrahedra that strongly depends on temperature and on the polarization conditions of the experiment.

In this work we measured the Raman modes corresponding to the vibration modes of the VO_4 tetrahedron in BiVO_4 over large temperature range at different light polarization geometries. We observed anomalies in the line-shape and in the frequency position of these Raman modes that suggest coupling between phonons of the same symmetry. We applied the coupled damped harmonic oscillators model to describe the observed phonon-phonon coupling for two different polarization conditions. Finally We studied the phonon-phonon coupling in a high temperature range from 10 K to 510 K across the phase transition.

EXPERIMENTAL METHODS

We investigated Raman spectra of BiVO_4 single crystals over a large temperature range. The Raman spectrometer InVia from Renishaw in backscattering configuration with a microscope, 50x objective was used. For all measurements, we used 633 nm (1.96 eV) laser excitation. We use the Porto's notation $i(jk)l$ to label the different polarization geometries, where i and l correspond to the propagation direction and j and k the polarization direction with respect to the crystallographic axis. Linkam temperature cell THMS600 was used to cover temperatures from 80 K to 500 K. The helium flow cryostat Microstat from Oxford Instruments was used to cover the low temperature range from 10 K to 300 K.

The crystal structure of BiVO_4 is tetragonal at high temperature with a phase transition at 523 K to monoclinic. Fig. 1 (a) shows the tetragonal unit cell with 4-fold rotational axis along $[001]$. In the low-temperature monoclinic phase, the 4-fold rotational axis becomes a 2-fold rotational axis, the so called principle axis. For this study we used a single with the surface orientation (110) . The view on the (110) surface is given in Fig. 1 (b) in which the principal axis is labeled with c and the $[1\bar{1}0]$ -axis with b' . The direction $[110]$ pointing out of the surface plane is labeled with a' . From standard symmetry analysis, we expect 8 phonon modes of A_g symmetry and 10 phonon modes of B_g symmetry in the monoclinic phase.[34, 35]

The Raman (Stokes) scattering intensity is correlated to the imaginary part of the susceptibility χ''

$$S(\omega) \propto \chi''(\omega)[n(\omega) + 1], \quad (1a)$$

where n is the phonon population factor given by the Bose thermal factor $n(\omega) = (e^{\hbar\omega/kT} - 1)^{-1}$ and T is the absolute temperature of the sample. All presented data

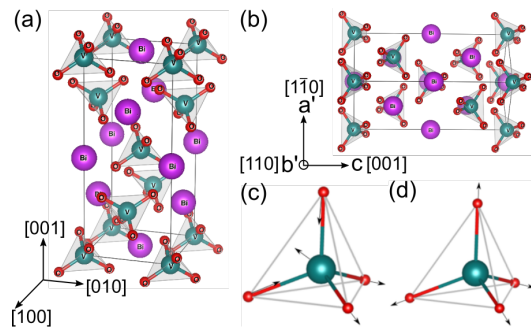


Figure 1. Schematic representation of (a) the tetragonal unit cell of bismuth vanadate and (b) view on the (001) surface. Visualization of the symmetries of the atomic vibrations of the oxygen tetrahedron corresponding to (c) the A_g^7 and (d) the A_g^8 .

have been divided by the thermal Bose factor $n(\omega) + 1$ so that they are directly proportional to the imaginary part of the susceptibility. The description of the Raman scattering intensity strongly depends on the model chosen for the susceptibility.

THEORETICAL METHODS

In the following the coupled damped harmonic oscillators (coupled oscillators) model is explained. The basic concept has been developed by Barker and Hopfield.[28] Fig. 2 shows the mechanical model for a system of two coupled phonons. Each phonon is described as a damped harmonic oscillator with an effective mass m , spring constant k and damping coefficient Γ . The two masses α and β are mechanically connected by an additional spring $k_{\alpha\beta}$ and dashpot $\Gamma_{\alpha\beta}$.

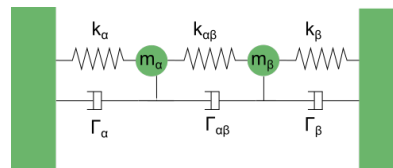


Figure 2. Mechanical model of two damped harmonic oscillators α and β described by spring constants k_α , k_β and the damping coefficients $\Gamma_\alpha, \Gamma_\beta$. The coupling is complex and given by the coupling spring constant $k_{\alpha\beta}$ and the damping coefficient $\Gamma_{\alpha\beta}$.

The Green's function may be written as $G^{-1} = g = -\omega^2 \mathbf{I}_2 + i\omega \mathbf{\Gamma} + \mathbf{K}$ in which \mathbf{I}_2 being the unit matrix and \mathbf{K} and $\mathbf{\Gamma}$ being restoring force and damping matrices. Using the Green's function formalism a system of two coupled damped harmonic oscillators[18, 19] is defined by

$$\begin{bmatrix} \omega_\alpha^2 - \omega^2 + i\omega\Gamma_\alpha & \Delta^2 + i\omega\Gamma_{\alpha\beta} \\ \Delta^2 + i\omega\Gamma_{\alpha\beta} & \omega_\beta^2 - \omega^2 + i\omega\Gamma_\beta \end{bmatrix} \begin{bmatrix} G_{\alpha\alpha} & G_{\alpha\beta} \\ G_{\alpha\beta} & G_{\beta\beta} \end{bmatrix} = \begin{bmatrix} 1 & 0 \\ 0 & 1 \end{bmatrix} \quad (1b)$$

The parameters Δ , Γ_α , Γ_β and $\Gamma_{\alpha\beta}$ are frequency independent. The effective mass m is set to unity. The coupling is described by Δ and $\Gamma_{\alpha\beta}$ which is the force constant of the spring and the damping coefficient of the dashpot connecting the two oscillators. Δ and $\Gamma_{\alpha\beta}$ must be constraint by $\det(K), \det(\Gamma) \geq 0$. [36] This means that the coupling cannot be arbitrary large. The frequencies ω_α and ω_β correspond to the eigenfrequencies of the uncoupled phonons. The eigenfrequency squared is equal to the spring constant divided by the effective mass m , $\omega_{\alpha/\beta}^2 = k_{\alpha/\beta}/m_{\alpha/\beta}$. Γ_α and Γ_β are the damping coefficient of the uncoupled vibration modes α and β .

Equation 1b is solved to give the following Green's functions coefficients:

$$G_{\alpha\alpha} = (\omega_\beta^2 - \omega^2 + i\omega\Gamma_\beta)/D \quad (1c)$$

$$G_{\alpha\beta} = -(\Delta^2 + i\omega\Gamma_{\alpha\beta})/D \quad (1d)$$

$$G_{\beta\beta} = (\omega_\alpha^2 - \omega^2 + i\omega\Gamma_\alpha)/D \quad (1e)$$

where $D = (\omega_\alpha^2 - \omega^2 + i\omega\Gamma_\alpha)(\omega_\beta^2 - \omega^2 + i\omega\Gamma_\beta) - (\Delta^2 + i\omega\Gamma_{\alpha\beta})^2$.

Equation 1b allows arbitrary choice of diagonalization and can produce an infinite number of solutions. [37] Some physical assumptions have to be made to filter reasonable solutions. Many authors [36, 38] proposed to make the assumptions on the complex coupling of modes in which the two limiting cases occur for only real coupling ($\Gamma_{\alpha\beta} = 0$) and only imaginary coupling ($\Delta = 0$). The parameters obtained in the two cases are entirely different as well as the physical interpretation, see supplementary information. In this work, we suggest to make use of the temperature dependent data as well as the polarization dependent data to find an unique solution to the coupled oscillators model.

Using matrix notation, the complex susceptibility $\chi(\omega)$ for coupled oscillators model is given by $\chi(\omega) = \tilde{P} \cdot G \cdot P$ in which P and \tilde{P} are one column and one row vectors. The imaginary part of the complex susceptibility $\chi''(\omega)$ is then given by

$$\chi''(\omega) = -Im[P_\alpha^2 G_{\alpha\alpha}(\omega) + 2P_\alpha P_\beta G_{\alpha\beta}(\omega) + P_\beta^2 G_{\beta\beta}(\omega)], \quad (1f)$$

P_α , P_β being the oscillator strengths of the vibration mode α and β and χ'' is proportional to the intensity of the Raman spectrum.

EXPERIMENTAL RESULTS

First, we discuss the evidences for coupling phenomena in the high-frequency Raman spectrum of BiVO₄. Raman spectra showing all 8 Raman modes of A_g symmetry are shown in the supplementary information. For most of these Raman modes, the eigenfrequency does not dependent on the polarization conditions chosen in the experiment, however this is different for the high-frequency A_g^7

mode that shows coupling signatures with the A_g^8 mode. Fig. 1 (b) shows A_g^7 near 705 cm⁻¹ and A_g^8 at 830 cm⁻¹ measured at room temperature. The symmetries of the atomic vibrations corresponding to the polar A_g^7 and the non-polar A_g^8 mode are shown in Figs. 1 (c) and (d), respectively.

Fig. 3 compares the phonon modes A_g^7 and A_g^8 measured at (a) 200 K and (b) room temperature for two polarization geometries. The first observation we made on the raw data is that the central frequency of the A_g^7 depends on the polarization geometry, $\Delta\omega = 8$ and 10 cm⁻¹ for 200 and 300 K, respectively. Second, at 300 K and for the polarization $b'(a'a')\bar{b}'$ (brown spectrum in Fig.3 (b)), we see additional intensity in between the two Raman modes.

Lorentz model fails to reproduce the experimental data, see dotted line. At 200 K the Lorentz model only partly converges with the data by assuming non physical behavior: different A_g^7 eigenfrequency for different polarization conditions. The fitting parameters are given in Table I. At 300 K the two Lorentzian peaks fit even fails to identify the A_g^7 phonon mode, if the frequency is not fixed. There are two reasons for that; first the line-shape of the A_g^7 is more asymmetric at higher temperatures and there is significant intensity background in between the two modes. Overall it is clear that the Lorentz model cannot be used for the Raman interpretation since it delivers falsified results. While the eigenfrequency of the A_g^8 mode almost matches for both polarization geometries, the eigenfrequency of the A_g^7 mode is different from one polarization geometry to the other by almost 1.2 %. This is rather unexpected, since mode frequency should be independent upon polarization and can only be explained by the coupled oscillator model.

Now we will discuss the fits using the coupled oscillators model. For the coupled oscillators model we imposed the same eigenfrequency and the damping coefficient for both polarization geometries. Further, we assumed the real part of the coupling parameter Δ to be zero. For the A_g^8 phonon mode, there is little difference between the classical Lorentzian and the coupled oscillators models. The overall line-shape is well described by both models and the frequency position as well as the damping coefficient of the A_g^8 mode is nearly identical for the both models. The major improvement is found for the A_g^7 mode at 300 K. The coupled oscillators model succeeds to describe the asymmetry in the line-shape of the A_g^7 mode as well as the increased background intensity in between the two modes. This is especially true for the $b'(a'a')\bar{b}'$ polarization geometry. The coupling coefficients are listed in Table I, they vary from one polarization geometry to the other. For $b'(cc)\bar{b}'$, the imaginary part of the coupling parameter Γ_{78} is positive which correspond to a repulsion of the two phonon modes involved in the coupling. In contrast, for $b'(a'a')\bar{b}'$, the imaginary part Γ_{78} is negative leading to an attraction of the two phonon modes.

We further study the temperature dependence of phonon-phonon more systematically. Fig. 4 (a) shows the A_g^7 and the A_g^8 mode measured at temperatures

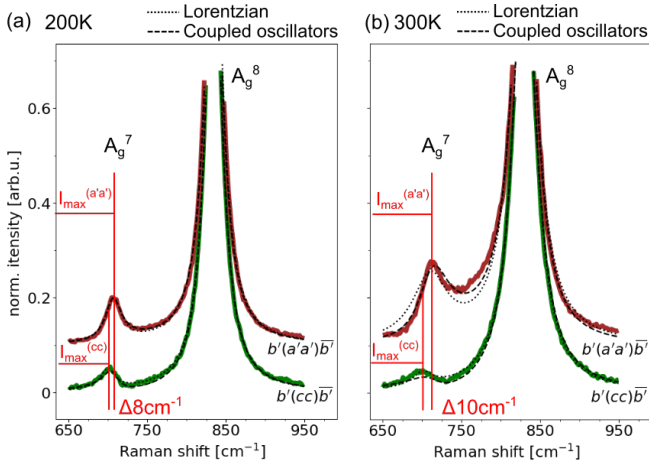


Figure 3. Raman spectra of the high-frequency A_g^7 and A_g^8 modes measured at different polarization geometries $b'(cc)\bar{b}'$ and $b'(a'a')\bar{b}'$ at (a) 200 K and (b) 300 K with a 1.96 eV excitation. Dashed lines show the fit assuming two Lorentzian oscillators in black and coupled oscillators model in blue. The fitting parameters are given in Table I.

Table I. Comparison of fitting parameters between the classical Lorentzian model and coupled oscillators model at 200 K and 300 K. Here, the real part of the coupling Δ is fixed to zero. The eigenfrequencies ω and damping coefficients Γ are given in units of cm^{-1} .

	200K		300K	
	$b'(a'a')\bar{b}'$	$b'(cc)\bar{b}'$	$b'(a'a')\bar{b}'$	$b'(cc)\bar{b}'$
Lorentzian model				
ω_7	708	700	711 (fixed)	701 (fixed)
Γ_7	24	22	54	31
ω_8	834	835	830	830
Γ_8	26	26	36	34
Coupled oscillators model				
ω_7	706		712	
Γ_7	25.5		47.0	
ω_8	835		831	
Γ_8	26.2		34.9	
Γ_{78}	-5.3	12.3	-15.0	22.4

ranging from 10 K up to phase transition at 523 K for the polarization geometries $b'(a'a')\bar{b}'$. By increasing the temperature we observe typical effects: the modes shift and broadening with temperature. The A_g^8 mode clearly shifts to lower frequencies with increasing temperatures whereas the A_g^7 seemingly shift to higher frequencies. Also we can directly see the evolution of phonon-phonon coupling. At low temperatures, the two Raman modes are well isolated whereas at higher temperature additional intensity develops in between the modes. The additional intensity increases with increasing temperatures with respect to the intensity contribution from the individual modes. That is why, we expect a strong temperature dependence of the coupling parameter.

Fig. 4 (b) shows a zoomed spectral range with the A_g^7

mode measured with $b'(cc)\bar{b}'$ polarization. In this light polarization the A_g^7 mode becomes extremely weak compared to the A_g^8 mode while approaching the phase transitions. At temperatures above 470 K, the A_g^7 mode is no longer visible in the raw data, see also the supplementary information. Surprisingly, the A_g^7 mode shifts to lower frequencies with increasing temperatures which contradicts the measurement for $b'(a'a')\bar{b}'$ shown in Fig. 4 (a). A phonon-phonon coupling model is required to explain this unconventional behavior.

The black dashed lines in Fig. 4 are fits based on the coupled oscillators model. For both polarization geometries we find a good agreement between the model and experiment. As mentioned in the methods section, the coupled oscillators model is overparameterized so that assumptions on the fitting parameters have to be made. We assumed i) the coupling parameter Δ to be zero, ii) the individual damping Γ_7, Γ_8 to increase linearly with temperature at a constant slope of 0.1 and $0.08 \text{ cm}^{-1} \text{ K}^{-1}$, respectively as expected for two-phonon decay and iii) the eigenfrequency of the A_g^7 mode to be constant as a function of temperature for the light polarization $b'(a'a')\bar{b}'$. As a final element we implemented a *weight* equal to the inverse of the intensity in the minimization algorithm. The implementation of a *weight* compensates for the huge intensity difference between the A_g^7 and the A_g^8 mode and is introduced as a multiplication factor so that $weight \cdot (data - fit)^2$ is minimized. This non-standard implementation in the minimization algorithm was key to find fitting solutions for the data measured at $b'(cc)\bar{b}'$ polarization and at high temperatures. The intensity difference is not as drastic for the $b'(a'a')\bar{b}'$ light polarization, so that in this case the *weight* was set to one.

Fig. 5 (a) shows the eigenfrequency ω_8 of the A_g^8 mode extracted from the fits shown in Fig.4 as a function of temperature for the two polarization geometries. The data points above the phase transition are included and symbolized with a cross. The eigenfrequency ω_8 strongly decreases with increasing temperature as it is visible in the raw data shown in Fig.4. Across the phase transition at $T_c = 510 \text{ K}$, the change in the eigenfrequency is continuous. This is expected for the second-order phase transition, but the slope clearly changes at the phase transition.

Fig. 5 (b) shows the eigenfrequency ω_7 of the A_g^7 as a function of temperature for the two polarization geometries. For the polarization geometry $b'(cc)\bar{b}'$, the eigenfrequency of the A_g^7 is constant over a large temperature range, before the values slightly increases while approaching the phase transition. A constant temperature trend of eigenfrequency ω_7 is only obtained by the coupled oscillators model, see also Lorentzian fitting as a function of temperature in the supplementary information. Even though we do not have data at temperatures above 470 K, the change in the eigenfrequency seems to be continuous similar to the discussion for the eigenfrequency of the A_g^8 mode.

To find a reliable temperature trend for the coupling parameter we assumed the eigenfrequency ω_7 to be independent on temperature for the second polarization geometry $b'(a'a')\bar{b}'$. The intensity of the mode is rela-

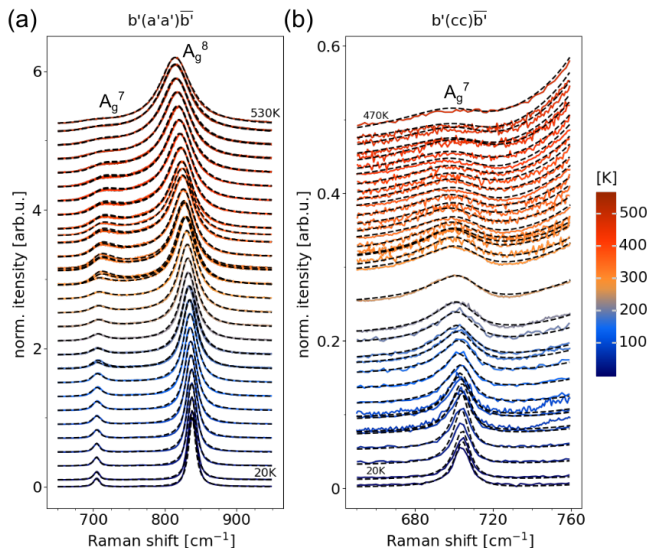


Figure 4. Coupled oscillators model applied to the Raman modes A_g^7 and A_g^8 at different temperatures for the (a) polarization geometry $b'(a'a')\bar{b}'$ and (b) $b'(cc)\bar{b}'$. Here, the real part of the coupling Δ is assumed to be zero. The damping of the individual oscillators Γ_7 and Γ_8 is assumed to increase linear with temperature. Only for polarization geometry $b'(a'a')\bar{b}'$, eigenfrequency ω_7 of the A_g^7 mode is assumed to be constant.

tively low therefore constraining it's frequency substantially improved the reliability of the fit. This is fully consistent with lattice dynamics where in non-polar crystals the ω_7 should be polarization independent. Therefore the ω_7 was set to 705 cm^{-1} , same as the average frequency found in the $b'(cc)\bar{b}'$ polarization direction. While the eigenfrequency of the A_g^8 mode is robust against different modeling approaches, coupled oscillators model succeeds to deliver physical results for the A_g^7 mode, where experimental data are reproduced with the same eigenfrequency for both polarization directions in the entire measured temperature range.

Fig. 6 shows the coupling parameter Γ_{78} as a function of temperature for the polarization geometries $b'(cc)\bar{b}'$ and $b'(a'a')\bar{b}'$, respectively. In the polarization geometry $b'(cc)\bar{b}'$, the coupling parameter is positive and increases continuously with increasing temperatures below 400 K, see red circles in Figure 6. On the other hand the Γ_{78} for $b'(cc)\bar{b}'$ has an opposite trend in the same temperature range. The overall magnitude of the coupling increases, but the sign is negative, see green triangles in Figure 6. The data between 160 K and 300 K have been measured at a later experiment and show a small offset to overall temperature trend. Overall we have a precise control over the phonon-phonon coupling, where the coupling strength is set by temperature and the coupling sign by the light polarization.

Now we discuss the coupling behavior near the phase transition. When going from monoclinic to tetragonal the phonon symmetries change, along with the selection rules. The A_g^7 changes its symmetry to a B_g symmetry

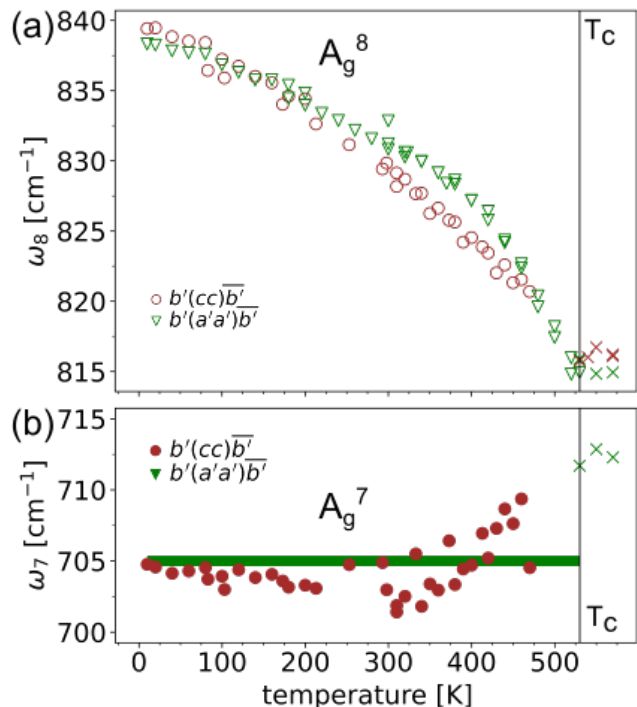


Figure 5. Fitting parameters of the coupled oscillators model applied to the Raman modes A_g^7 and A_g^8 as a function of temperature: eigenfrequency for the two polarization geometries of (a) the low intensity A_g^7 mode and (b) of the A_g^8 mode.

while the A_g^8 remains of A_g symmetry. As a consequence, we expect no coupling between these two phonons in the high-temperature tetragonal phase. This is reflected in change of the temperature trend found the coupling parameter for the light polarization $b'(a'a')\bar{b}'$ in which the coupling parameter decreases while approaching the phase transition.

The situation is slightly different for the other light polarization $b'(cc)\bar{b}'$, where only modes of A_g symmetry are allowed in the tetragonal phase. [35] Therefore, the Raman intensity of the A_g^7 mode gradually decreases with temperature until it disappears in the tetragonal phase. This is nicely observed in the waterfall plot shown in Fig 4 (b). The ratio of the relative intensities is plotted in the supplementary information. Therefore the symbols for Γ_{78} at $b'(cc)\bar{b}'$ are missing in Figure 6. Overall we in BiVO_4 we find a beautiful demonstration how the change of phonon symmetries influences phonon-phonon coupling. We confirm that only phonon modes of the same symmetry can couple as predicted by Chaves *et al.* [15].

CONCLUSION

In BiVO_4 we studied coupling between two optical phonons with the A_g symmetry. We show that the phonon-phonon coupling causes the asymmetric line-shapes of the A_g^7 and A_g^8 mode at temperatures above

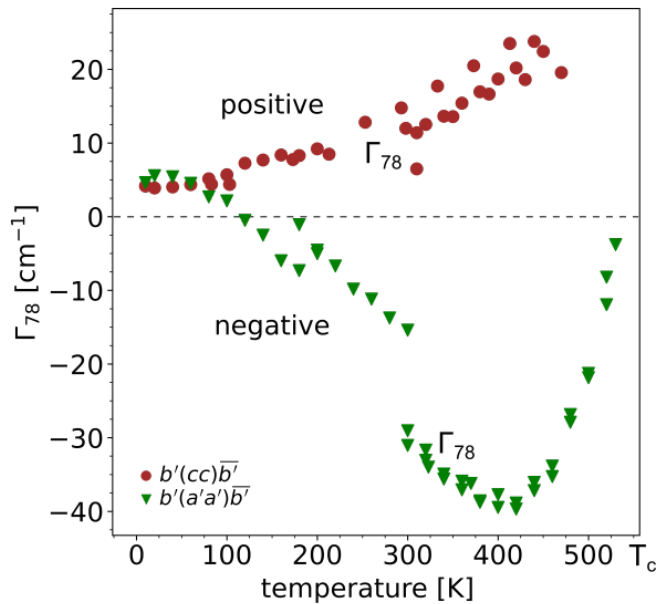


Figure 6. Coupling parameter Γ_{78} as a function of temperature for the polarization geometry $b'(cc)\bar{b}'$ and $b'(a'a')\bar{b}'$. Because the intensity of the A_g^7 mode diminishes while approaching the phase transition, there are no data for Γ_{78} at temperatures above 470 K in case of the $b'(cc)\bar{b}'$ polarization.

100 K. Depending on the polarization geometry, the sign of coupling parameter is either positive or negative referring to either repulsion or attraction of phonon modes. The coupling strength, expressed in the absolute value of the coupling parameter, increases with increasing temperatures. At temperatures above 400 K, the coupling strength decreases for the $b'(a'a')\bar{b}'$ polarization geometry. This is explained by the change in symmetry of the A_g^7 mode, which leads to decoupling of the two phonon modes above the phase transition temperature.

ACKNOWLEDGMENTS

CH acknowledges funding from the Fond National de la Recherche under Project PRIDE/15/10935404. This research was funded in whole, or in part, by the Luxembourg National Research Fund (FNR), grant reference [INTER/MERA20/14995416/SWIPE]. For the purpose of open access, and in fulfilment of the obligations arising from the grant agreement, the author has applied a Creative Commons Attribution 4.0 International (CC BY 4.0) license to any Author Accepted Manuscript version arising from this submission.

-
- [1] R. J. Meier, On art and science in curve-fitting vibrational spectra, *Vibrational Spectroscopy* **39**, 266 (2005).
 - [2] Y. Chen and L. Dai, Automated decomposition algorithm for Raman spectra based on a Voigt line profile model, *Applied Optics* **55**, 4085 (2016).
 - [3] F. Alsmeyer and W. Marquardt, Automatic generation of peak-shaped models, *Applied Spectroscopy* **58**, 986 (2004).
 - [4] B. O. Mysen, L. W. Finger, D. Virgo, and S. F. A., Curve-fitting of raman spectra of silicate glasses, *American Mineralogist* **67**, 686 (1982).
 - [5] G. Gouadec and P. Colomban, Raman spectroscopy of nanomaterials: How spectra relate to disorder, particle size and mechanical properties, *Progress in Crystal Growth and Characterization of Materials* **53**, 1 (2007).
 - [6] R. Cuscó, E. Alarcón-Lladó, J. Ibáñez, L. Artús, J. Jiménez, B. Wang, and M. J. Callahan, Temperature dependence of raman scattering in zno, *Physical Review B* **75**, 165202 (2007).
 - [7] U. T. Schwarz and M. Maier, Asymmetric raman lines caused by an anharmonic lattice potential in lithium niobate, *Physical Review B* **55**, 11041 (1997-05-01).
 - [8] K. Adu, Q. Xiong, H. Gutierrez, G. Chen, and P. Eklund, Raman scattering as a probe of phonon confinement and surface optical modes in semiconducting nanowires, *Applied Physics A* **85**, 287 (2006).
 - [9] R. J. Nemanich, S. A. Solin, and R. M. Martin, Light scattering study of boron nitride microcrystals, *Physical Review B* **23**, 6348 (1981).
 - [10] V. I. Korepanov and H. O. Hamaguchi, Quantum-chemical perspective of nanoscale Raman spectroscopy with the three-dimensional phonon confinement model, *Journal of Raman Spectroscopy* **48**, 842 (2017).
 - [11] E. H. Martins Ferreira, M. V. O. Moutinho, F. Stavale, M. M. Lucchese, R. B. Capaz, C. A. Achete, and A. Jorio, Evolution of the raman spectra from single-, few-, and many-layer graphene with increasing disorder, *Physical Review B* **82**, 125429 (2010).
 - [12] M. Huang, H. Yan, C. Chen, D. Song, T. F. Heinz, and J. Hone, Phonon softening and crystallographic orientation of strained graphene studied by Raman spectroscopy, *Proceedings of the National Academy of Sciences of the United States of America* **106**, 7304 (2009).
 - [13] R. Lehnert, P. Hendra, N. Everall, and N. Clayden, Comparative quantitative study on the crystallinity of poly(tetrafluoroethylene) including raman, infra-red and ^{19}F nuclear magnetic resonance spectroscopy, *Polymer* **38**, 1521 (1997).
 - [14] J. F. Scott, Evidence of coupling between one- and two-phonon excitations in quartz, *Physical Review Letters* **21**, 907 (1968).
 - [15] A. Chaves, R. S. Katiyar, and S. P. Porto, Coupled modes with A_1 symmetry in tetragonal BaTiO_3 , *Physical Review B* **10**, 3522 (1974).
 - [16] J. F. Scott, Hybrid Phonons and Anharmonic Interactions in AlPO_4 , *Physical Review Letters* **24**, 1107 (1970).
 - [17] J. F. Scott, Soft-mode spectroscopy: Experimental studies of structural phase transitions, *Reviews of Modern Physics* **46**, 83 (1974).
 - [18] C. Y. She, T. W. Broberg, L. S. Wall, and D. F. Edwards, Effect of proton-phonon coupling on the ferroelectric mode in KH_2PO_4 , *Physical Review B* **6**, 1847 (1972).
 - [19] R. S. Katiyar, J. F. Ryan, and J. F. Scott, Proton-phonon coupling in CsH_2AsO_4 and KH_2AsO_4 , *Physical Review B* **4**, 2635 (1971).

- [20] D. L. Rousseau and S. P. S. Porto, Auger-like resonant interference in raman scattering from one- and two-phonon states of BaTiO_3 , *Physical Review Letters* **20**, 1354 (1968).
- [21] J. W. Ager, W. Walukiewicz, M. McCluskey, M. A. Plano, and M. I. Landstrass, Fano interference of the raman phonon in heavily boron-doped diamond films grown by chemical vapor deposition, *Applied Physics Letters* **66**, 616 (1995).
- [22] B. G. Burke, J. Chan, K. A. Williams, Z. Wu, A. A. Puzos, and D. B. Geohegan, Raman study of fano interference in p-type doped silicon, *Journal of Raman Spectroscopy* **41**, 1759 (2010), 0910.5244 [cond-mat, physics:physics].
- [23] V. Magidson and R. Beserman, Fano-type interference in the raman spectrum of photoexcited si, *Physical Review B* **66**, 195206 (2002).
- [24] U. Fano, Effects of configuration interaction on intensities and phase shifts, *Physical Review* **124**, 1866 (1961).
- [25] G. Breit and E. Wigner, Capture of slow neutrons, *Physical Review* **49**, 519 (1936).
- [26] S. D. M. Brown, A. Jorio, P. Corio, M. S. Dresselhaus, G. Dresselhaus, R. Saito, and K. Kneipp, Origin of the breit-wigner-fano lineshape of the tangential G -band feature of metallic carbon nanotubes, *Physical Review B* **63**, 155414 (2001).
- [27] G. Gordeev, A. Setaro, M. Glaeske, S. Jürgensen, and S. Reich, Doping in covalently functionalized carbon nanotubes: A Raman scattering study, *Physica Status Solidi (B)* **253**, 2461 (2016).
- [28] A. S. Barker and J. J. Hopfield, Coupled-optical-phonon-mode theory of the infrared dispersion in BaTiO_3 , SrTiO_3 , and KTaO_3 , *Physical Review* **135**, A1732 (1964).
- [29] A. Zawadowski and J. Ruvalds, Indirect Coupling and Antiresonance of Two Optic Phonons, *Physical Review Letters* **24**, 1111 (1970).
- [30] A. Scalabrin, A. S. Chaves, D. S. Shim, and S. P. Porto, Temperature dependence of the A1 and E optical phonons in BaTiO_3 , *Physica Status Solidi (B)* **79**, 731 (1977).
- [31] N. Lagakos and H. Z. Cummins, Preliminary observation of a central peak in the light-scattering spectrum of KH_2PO_4 , *Physical Review B* **10**, 1063 (1974).
- [32] D. G. Boziniš and J. P. Hurrell, Optical modes and dielectric properties of ferroelectric orthorhombic KNbO_3 , *Physical Review B* **13**, 3109 (1976).
- [33] G. Benyuan, M. Copic, and H. Z. Cummins, Soft acoustic mode in ferroelastic BiVO_4 , *Physical Review B* **24**, 4098 (1981).
- [34] L. P. Avakyants, A. V. Chervyakov, V. S. Gorelik, and P. P. Sverbil', Inelastic light scattering near the ferroelectric phase-transition point in bismuth vanadate crystals, *Journal of Russian Laser Research* **25**, 535 (2004).
- [35] J. Pellicer-Porres, D. Vázquez-Socorro, S. López-Moreno, A. Muñoz, P. Rodríguez-Hernández, D. Martínez-García, S. N. Achary, A. J. E. Rettie, and C. B. Mullins, Phase transition systematics in BiVO_4 by means of high-pressure-high-temperature raman experiments, *Physical Review B* **98**, 214109 (2018).
- [36] Y. Takagi, Coupled modes analysis of raman spectra: Application to the case of a KH_2PO_4 crystal in the paraelectric phase, *Ferroelectrics* **46**, 245 (1983).
- [37] R. P. Lowndes, N. E. Tornberg, and R. C. Leung, Ferroelectric mode and molecular structure in the hydrogen-bonded ferroelectric arsenates and their deuterated isomorphs, *Physical Review B* **10**, 911 (1974).
- [38] V. Mazzacurati, G. Signorelli, and M. Sampoli, Indirect coupling of the soft optic phonon in KH_2PO_4 , *Journal of Raman Spectroscopy* **4**, 339 (1976).
- [39] M. A. F. Scarparo, R. S. Katiyar, R. Srivastava, and S. P. S. Porto, Evidence of non-linear behaviour of soft modes in crystals with kdp structure, *Physica Status Solidi (b)* **90**, 543 (1978).
- [40] I. P. Kaminow and T. C. Damen, Temperature dependence of the ferroelectric mode in KH_2PO_4 , *Physical Review Letters* **20**, 1105 (1968).
- [41] G. Burns and B. A. Scott, Lattice modes in ferroelectric perovskites: PbTiO_3 , *Physical Review B* **7**, 3088 (1973).
- [42] A. Chaves, R. S. Katiyar, and S. P. S. Porto, Coupled modes with a1 symmetry in tetragonal BaTiO_3 , *Physical Review B* **10**, 3522 (1974).
- [43] M. S. Liu, L. A. Bursill, S. Prawer, and R. Beserman, Temperature dependence of the first-order raman phonon line of diamond, *Physical Review B* **61**, 3391 (2000).
- [44] P. G. Klemens, Anharmonic decay of optical phonons, *Physical Review* **148**, 845 (1966).
- [45] K.-R. Zhu, M.-S. Zhang, Q. Chen, and Z. Yin, Size and phonon-confinement effects on low-frequency raman mode of anatase TiO_2 nanocrystal, *Physics Letters A* **340**, 220 (2005).
- [46] J. E. Spanier, R. D. Robinson, F. Zhang, S.-W. Chan, and I. P. Herman, Size-dependent properties of CeO_{2-y} nanoparticles as studied by raman scattering, *Physical Review B* **64**, 245407 (2001).
- [47] D. Wang, B. Chen, and J. Zhao, Lattice vibration fundamentals of nanocrystalline anatase: Temperature-dependent study using micro-raman scattering spectroscopy, *Journal of Applied Physics* **101**, 113501 (2007).
- [48] J. Menéndez and M. Cardona, Temperature dependence of the first-order raman scattering by phonons in si, ge, and α -sn : Anharmonic effects, *Physical Review B* **29**, 2051 (1984).
- [49] R. J. Meier, On art and science in curve-fitting vibrational spectra, *Vibrational Spectroscopy* **39**, 266 (2005).
- [50] P. Zhou, K.-A. Wang, A. M. Rao, P. C. Eklund, G. Dresselhaus, and M. S. Dresselhaus, Raman-scattering studies of homogeneous K_3C_{60} films, *Physical Review B* **45**, 10838 (1992).

Modeling a polarization-dependent phonon-phonon coupling in the Raman spectrum of BiVO_4 over a large temperature range

Supplementary information

Christina Hill,^{1,2} Georgy Gordeev,² and Mael Guennou²

¹*Materials Research and Technology Department,*

Luxembourg Institute of Science and Technology, 41 rue du Brill, L-4422 Belvaux, Luxembourg

²*Department of Physics and Materials Science, University of Luxembourg, 41 rue du Brill, L-4422 Belvaux, Luxembourg*

CONTENTS

Coupled damped harmonic oscillator and its coupling coefficients	2
Raman modes of A_g symmetry of monoclinic bismuth vanadate	3
Evidence for phonon-phonon mode coupling - Polarization dependent temperature trend of the A_g^7 mode (Lorentzian fitting)	4
Coupled oscillators model - Oscillator strengths	5

COUPLED DAMPED HARMONIC OSCILLATOR AND ITS COUPLING COEFFICIENTS

Fig. 1 shows the imaginary part of the susceptibility $\chi''(\omega)$ calculated from the Greens Formalism (a) assuming no coupling, (b) Δ is non-zero, (c) $\Gamma_{\alpha\beta}$ is positive and (d) $\Gamma_{\alpha\beta}$ is negative. In case of Δ and $\Gamma_{\alpha\beta}$ being zero, the maximum intensity appears at the eigen-frequencies ω_α and ω_β of the individual phonons and the line-shape of both phonon bands is symmetric, see Fig. 1 (a). For non-zero Δ , the maxima no longer appear at the eigen-frequencies (repulsion of modes) and there is an intensity transfer from the phonon mode α to β . Figs. 1 (c) and (d) show the imaginary part of the susceptibility assuming positive and negative $\Gamma_{\alpha\beta}$, respectively. For positive $\Gamma_{\alpha\beta}$ the two phonon modes are pushed apart. For negative $\Gamma_{\alpha\beta}$ the two phonon modes are attracted. For both pure real and pure imaginary coupling the line-shape of the phonon bands becomes asymmetric.

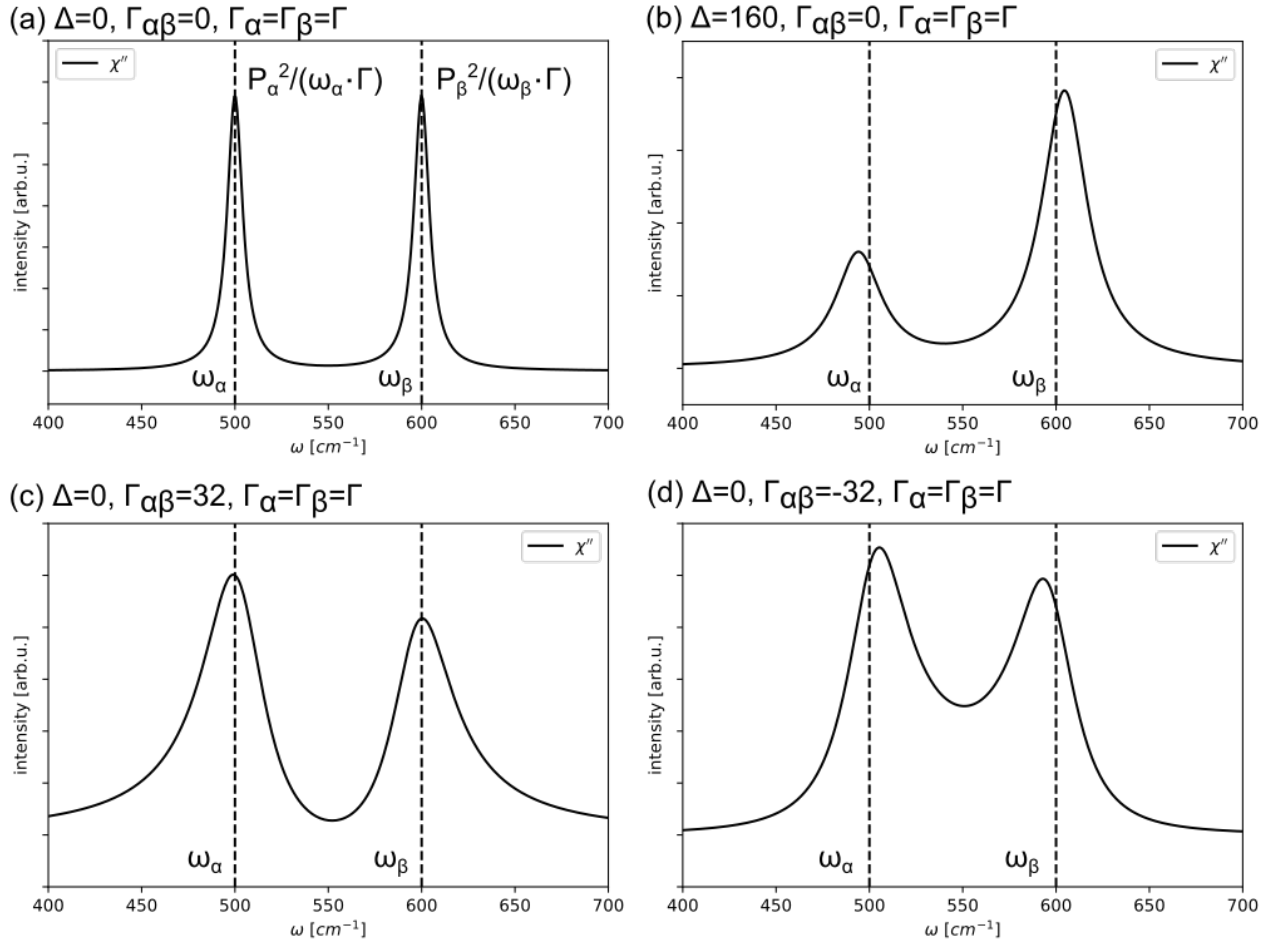


Figure 1: Imaginary part of the susceptibility $\chi''(\omega)$ calculated from Greens Formalism (a) without coupling assuming $\Delta = 0$ and damping $\Gamma_{\alpha\beta} = 0$ (b) Δ is non-zero (c) $\Gamma_{\alpha\beta}$ is positive (d) $\Gamma_{\alpha\beta}$ is negative

RAMAN MODES OF A_g SYMMETRY OF MONOCLINIC BISMUTH VANADATE

Fig.2 shows the Raman spectrum of BiVO_4 measured at $T=300\text{ K}$ with a laser excitation of 633 nm for the light polarizations $b'(cc)\bar{b}'$ and $b'(a'a')\bar{b}'$. All 8 A_g modes are successfully observed. The eigen-frequency is extracted at the maximum intensity of the different Raman bands. The eigen-frequencies are summarized in Table I for both polarizations. As expected, the eigen-frequencies of the individual Raman bands compares well between the two polarization conditions. For the A_g^7 mode, however, a significant difference in the eigen-frequency is observed from one polarization to the other. The origin for this difference is phonon-phonon coupling between the A_g^7 and A_g^8 mode which is discussed in the main paper.

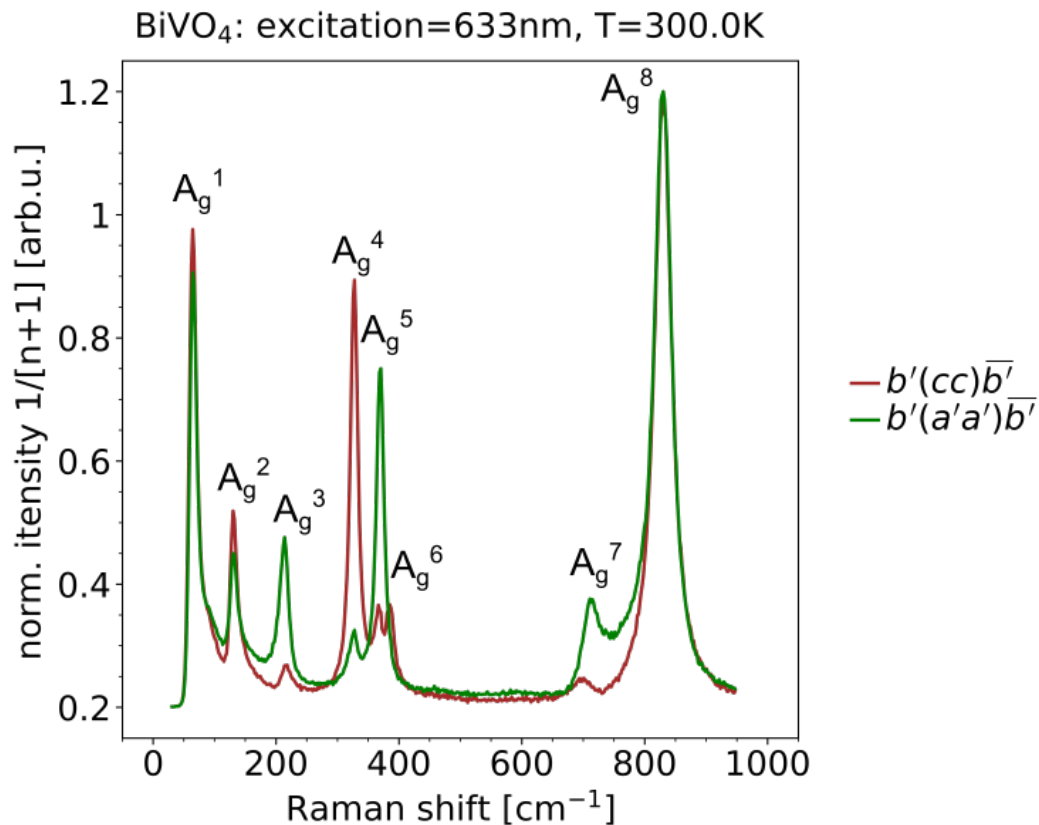


Figure 2: Raman spectra of the single crystal BiVO_4 measured at $T=300\text{ K}$ with a laser excitation of 633 nm for the light polarizations $b'(cc)\bar{b}'$ and $b'(a'a')\bar{b}'$. All spectra are normalized to the A_g^8 mode at 830 cm^{-1} .

Table I: Raman eigen-frequencies for both polarization geometries assigned to the active Raman modes with A_g symmetry. The eigen-frequencies are given in units of cm^{-1} .

Mode	$\omega_{(cc)}$	$\omega_{(a'a')}$
A_g^1	65	65
A_g^2	130	130
A_g^3	216	214
A_g^4	328	328
A_g^5	368	370
A_g^6	385	-
A_g^7	701	711
A_g^8	830	830

EVIDENCE FOR PHONON-PHONON MODE COUPLING - POLARIZATION DEPENDENT TEMPERATURE TREND OF THE A_g^7 MODE (LORENTZIAN FITTING)

Figs. 3 (a) and (b) show the high frequency A_g^7 and A_g^8 Raman modes measured as a function of temperature for the $b'(a'a')\bar{b}'$ and the $b'(cc)\bar{b}'$ polarization geometry, respectively. The A_g^8 mode clearly shifts to lower frequencies with increasing temperatures for both polarization geometries. The A_g^7 mode shift to higher frequencies for $b'(a'a')\bar{b}'$ whereas the temperature trend is opposite for $b'(cc)\bar{b}'$. The opposite temperature trend of the A_g^7 is surprising. In first approximation, there is no strong argument for the frequency position to be different between the two polarization geometries. This is a first indication that the A_g^7 strongly couples to the A_g^8 mode. Secondly, the line-shape of the A_g^7 is strongly asymmetric at temperatures above room temperature.

In a first attempt, A_g^7 and A_g^8 modes have been fitted with two Lorentzian functions. Because of the asymmetric line-shape of the A_g^7 mode at high temperatures, the Lorentzian function was used only from 10 K to 200 K for this mode. For the A_g^8 mode the Lorentzian function seem to provide a good fitting result up to the phase transition temperature. Figs. 3 (c) and (d) show the eigen-frequencies of the A_g^7 and A_g^8 mode as a function of temperature and polarization geometry, respectively. The eigen-frequency of the A_g^8 mode decreases with increasing temperature for both scattering geometries whereas the eigen-frequency of the A_g^7 has opposite temperature trend depending on the polarization geometry. The damping coefficients of both modes increase with temperatures as expected, see Figs. 3 (e) and (f). For temperatures above 100 K, the increase is nearly linear for both phonon modes and both scattering geometries. The linear fits are shown with black lines and the fitting equations are given in the corresponding plots. The linear temperature trend was used in the main paper to physical constrain the damping Γ_7 and Γ_8 of the A_g^7 and A_g^8 for the coupled oscillators model.

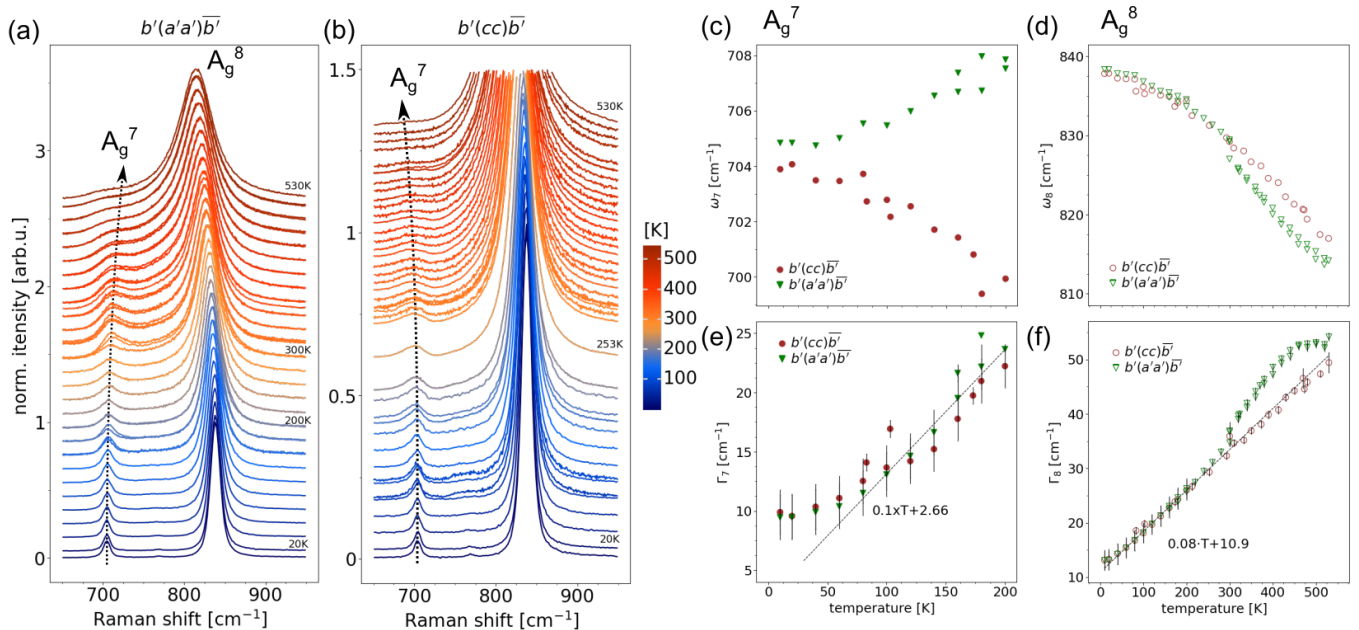


Figure 3: High frequency A_g^7 and A_g^8 Raman mode of monoclinic BiVO_4 measured for the two polarization geometries (a) $b'(a'a')\bar{b}'$ and (b) $b'(cc)\bar{b}'$ from 10 K up to 530 K with 633 nm laser excitation. (c) and (d) show the eigen-frequencies ω_7 , ω_8 and (e) and (f) the damping coefficient Γ_7 and Γ_8 obtained from the Lorentzian fitting. The damping coefficients increase nearly linear with increasing temperatures. The linear fits are shown with black lines and the fitting equations are provides in the plots.

COUPLED OSCILLATORS MODEL - OSCILLATOR STRENGTHS

Fig. 4 shows the ratio of the oscillator strengths P_7/P_8 as a function of the temperature for the polarization condition $b'(cc)\bar{b}'$ and $b'(a'a')\bar{b}'$. The ratio of the oscillator strengths P_7/P_8 decreases while approaching the phase transition for both polarization conditions. That is consistent with the observation on the raw data where the intensity of the A_g^7 is extremely weak at high temperatures at which the A_g^8 mode dominates.

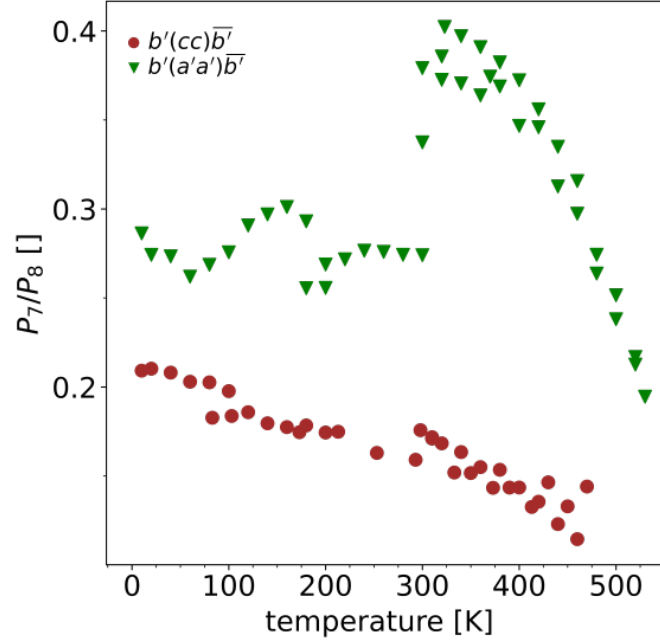


Figure 4: Oscillator strengths ratio P_7/P_8 as a function of temperature for the polarization condition $b'(cc)\bar{b}'$ and $b'(a'a')\bar{b}'$ obtained from the coupled oscillators model.